Fabrication of p-type Transparent (CuZn)O Thin Films by the Electrochemical Deposition Method

Mansoureh Keikhaei[*], *Masaya Ichimura*

Department of Engineering Physics, Electronics and Mechanics, Nagoya Institute of Technology, Gokiso, Showa, Nagoya 466-8555, Japan
[*]E-Mail: keykhaei@gmail.com, ichimura.masaya@nitech.ac.jp

Copper zinc oxide (CuZn)O thin films were fabricated on indium tin oxide-coated glass substrates using the cathodic electrochemical deposition method under various conditions. These included different temperatures, deposition times, and potentials. The deposition solution contained 1 mM $Cu(NO_3)_2$ and various concentrations of $Zn(NO_3)_2$. X-ray diffraction demonstrated that wurtzite structure for films deposited at 60°C, whereas samples that deposited at room temperature were amorphous. In the visible region, the samples exhibited high optical transmission, i.e., larger than 65%. Conductivity was found to be p-type by photoelectrochemical characterizations for the samples fabricated at room temperature. In contrast, the films fabricated at 60°C were n-type or close to intrinsic.

1. INTRODUCTION

Zinc Oxide (ZnO) has been receiving attention owing to its exclusive electrical and optical properties. It is a native n-type semiconductor with a direct band gap of around ~3.37 eV, and it possesses considerable exciton binding energy of 60 meV [1,2]. ZnO is an inexpensive and environmentally friendly material with high transparency in visible regions in its thin film form [1,3,4]. It is considered a promising material for surface acoustic wave devices and chemical sensors, as well as for a variety of novel applications such as lasers, blue LED, solar cells, and transparent conducting electrodes [3–6]. Zinc hydroxide ($Zn(OH)_2$) is an amphoteric compound with a band gap of around 5.65 eV. It can convert into ZnO by dehydration in air or under hydro(solvo)thermal conditions at raised temperatures [7–9].

For many ZnO-based devices, it is essential to fabricate stable, reliable, and reproducible p-

type films [10], which are necessary for PN junctions. However, fabrication of p-type ZnO is difficult because of the self-compensation effects by intrinsic defects, such as O vacancies and Zn interstitials and also because of the low solubility and high ionization energy of p-type dopants in ZnO [10–13]. It is known that Cu could be the potential p-type dopant candidate for ZnO [11], and Cu-doped ZnO has been synthesized by various techniques [5,6,14–19]. However, in most of these, the electrical properties, including conduction type, were not examined, and research confirming p-type conduction is limited. Several methods have been reported for synthesizing p-type (CuZn)O, e.g., sputtering [20,21], hydrothermal synthesis [22], spray deposition [2,4], atomic layer deposition [10], and electrochemical deposition (ECD) [12].

Among these methods, ECD is one of the most important techniques for developing semiconductor thin films because it is a simple and low-temperature process, it is low cost, and it is capable of broadscale fabrication on various substrates with both shape and size control. Ghahramanifard and colleagues reported ECD of p-type Cu-doped ZnO nanorods [12], and Lupan and colleagues reported ECD of n-type Cu-doped ZnO nanowires [23]. Thus, different conduction types have been reported previously. Moreover, only the deposition of nanorods or wires were reported and not the fabrication of flat thin films.

ECD of ZnO usually occurs at high temperatures (60°C—90°C) [12,23], and decreasing the deposition temperature causes the formation of an amorphous ZnO and/or $Zn(OH)_2$ [7]. To our knowledge, ECD of (CuZn)O at room temperature (RT) has not been reported thus far. In the research reported here, (CuZn)O thin films were fabricated by potentiostatic ECD on indium tin oxide (ITO)-coated glass substrates under different conditions. As shown, we succeeded in the deposition of transparent p-type (CuZn)O films at RT.

2. EXPERIMENTAL

For ECD, a standard three-electrode cell was used with a Hokutodenko HA151-B potentiostat/galvanostat. An ITO-coated glass substrate was used as the working electrode, a platinum sheet as the counter electrode, and an Ag/AgCl electrode as the reference electrode. We confirmed that ITO is stable in the deposition solution.

The ITO substrates were washed in acetone and purified water, and the deposited area was 1×1 cm^2. (CuZn)O thin films were fabricated by stirring in an aqueous electrolyte containing 1 mM $Cu(NO_3)_2 \cdot 6H_2O$ and various concentrations of $Zn(NO_3)_2 \cdot 6H_2O$ (5, 10, and 20 mM), at different potentials (−0.7, −0.75, and −0.8 V) and various deposition times (90, 150, 210, and 270 s). The deposition bath temperature was set at RT and 60°C. All samples were washed with deionized water and air dried subsequent to fabrication. For comparison, ZnO with a thickness of around 0.2 μm was deposited from a solution containing 0.1 M $Zn(NO_3)_2$ at 60°C with a current density of −1.2 mA and deposition time of 150 s.

Cyclic voltammetry (CV) was performed at a scan rate of 20 mV/s. Film-thickness values were obtained using an Accretech Surfcom-1400D profilometer. Scanning electron microscopy (SEM) images (5000 and 30000× magnifications) and Auger electron spectroscopy (AES) data were obtained using a JEOL JAMP-9500F field emission microprobe at a probe voltage of 10 keV. Cu/Zn ratios were

calculated using AES peak-to-peak intensity ratios of Cu and Zn. As a reference, commercially available standard CuO and ZnO chemicals were used. X-ray diffraction (XRD) was measured using a SmartLab X-ray diffractometer (Rigaku) with a CuKα radiation source. Optical transmittance measurement was conducted using a Jasco V-570 UV/VIS/NIR spectrometer. The ITO substrate was used as a reference. The photoelectrochemical (PEC) experiment was voltametrically measured in a three-electrode cell with the deposited films and Ag/AgCl as the working electrode and reference electrode, respectively, and a 0.1 M Na_2SO_4 aqueous solution as the electrolyte. For optical excitation of the films, an Abet Technologies 10500 solar simulator was used to intermittently radiate light (100 mW/cm^2) at 5 s intervals with a scan rate of 5 mV/s.

3. RESULTS

Fig. 1 illustrates the CV curves for four conditions: curves (a) and (b): pure 5 mM $Zn(NO_3)_2$ at RT and 60°C bath temperature, respectively; and curves (c) and (d): 1 mM $Cu(NO_3)_2$ and 5 mM $Zn(NO_3)_2$ at RT and 60°C, respectively. In curves (a) and (b), cathodic waves started to increase at −1.1 V. However, these waves shifted toward the positive direction with enhanced current density in the presence of copper ions in the solution in curves (c) and (d). The reduction in current densities at −1.2 V are −0.15, −0.5, −0.9, and −1.2 mA/cm^2 for curves (a), (b), (c), and (d), respectively. We associate all these reduction peaks to a reaction of nitrate ions, reaction (1):

$$NO_3^- + 2H_2O + 2e^- \rightarrow NO_2^- + 2OH^- \qquad (1)$$
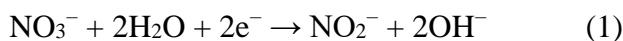
With the OH$^-$ ions thus generated, metal hydroxides are formed. In curves (c) and (d), the intensity of the cathode current increases with an increase in the bath temperature [24]. Metal oxides can be obtained from spontaneous dehydration of hydroxides at 60°C, e.g.,

$$Zn(OH)_2 \rightarrow ZnO + H_2O \qquad (2)$$
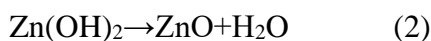
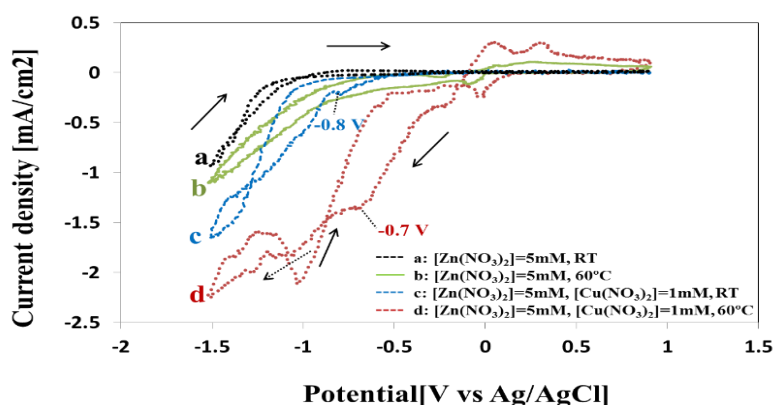However, these reactions will be much slower at RT.

Figure 1. CV of the solutions with 5 mM $Zn(NO_3)_2$ at (a) RT and (b) 60°C, with 5 mM $Zn(NO_3)_2$ and 1 mM $Cu(NO_3)_2$ at (c) RT and (d) 60°C.

Figs. 2(a) and (b) show the variation of film thickness with potential in the solution containing 1 mM $Cu(NO_3)_2$ and various concentrations of $Zn(NO_3)_2$ (5 mM and 20 mM) at RT. The figures for 10 mM $Zn(NO_3)_2$ are not shown here. There is no evident trend in the film-thickness variation with the increase in negative potential at deposition time of 150 s. The error bars show thickness fluctuation as a result of the non-uniformity or roughness. Considering the shift in CV curves shown in Fig. 1, less negative potential is suitable for 20 mM $Zn(NO_3)_2$ than for the lower $Zn(NO_3)_2$ concentration. Thus, −0.75 V was selected as the deposition potential for 5 mM and 10 mM $Zn(NO_3)_2$ and −0.7 V for 20-mM $Zn(NO_3)_2$.

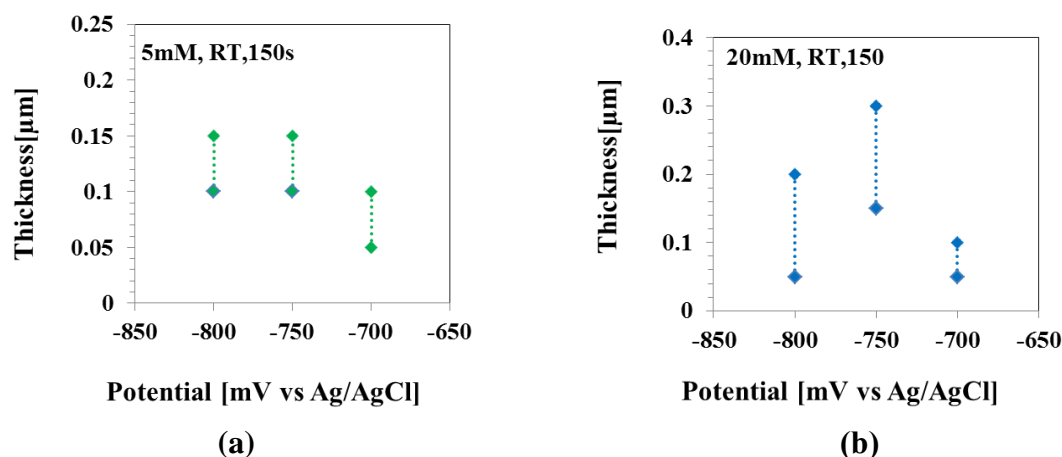**Figure 2.** Film thicknesses for the selected (CuZn)O films deposited at various potentials with 1 mM $Cu(NO_3)_2$ and (a) 5 mM and (b) 20 mM $Zn(NO_3)_2$ with a deposition time of 150 s.

The variation of film thickness with deposition time at 1 mM $Cu(NO_3)_2$ and various concentrations of $Zn(NO_3)_2$ (5 mM and 20 mM) at RT and 60°C is presented in Fig. 3(a)–(d). It is evident that as the deposition time increases, the thickness increases as well.
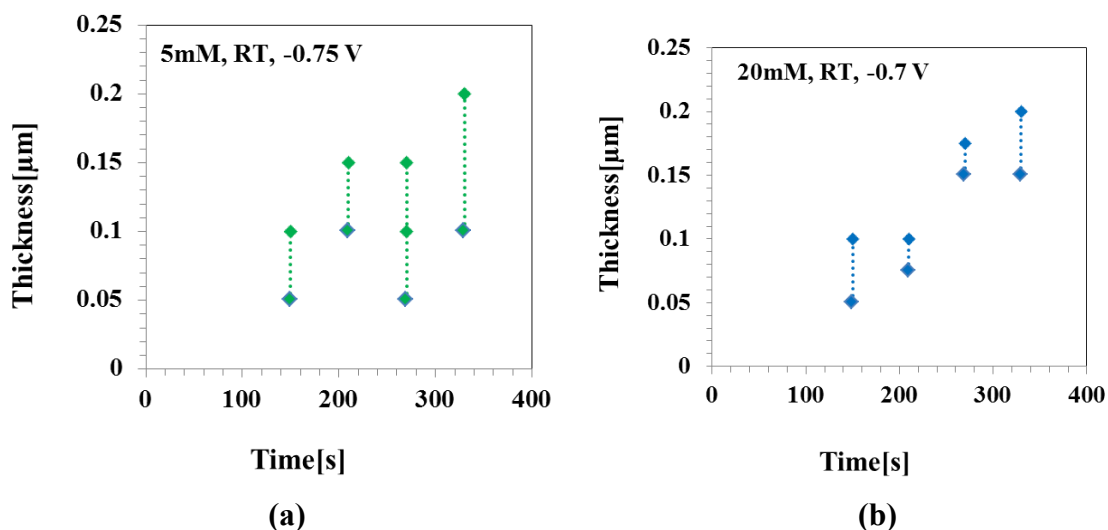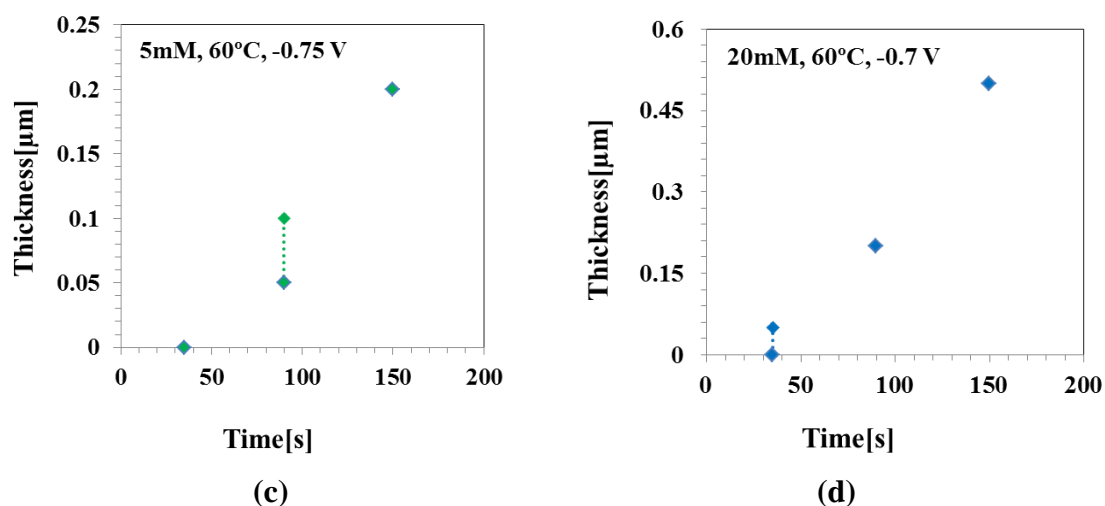
Figure 3. Dependence of the thickness on deposition time with 1 mM $Cu(NO_3)_2$ and various concentrations of $Zn(NO_3)_2$ at two bath temperatures. (a) and (b): RT, (c) and (d): 60°C.

Moreover, the films deposited at 60°C are significantly thicker than those deposited at RT. For 10 mM $Zn(NO_3)_2$, the thickness is around 0.1 µm, with 150 s deposition time at RT, and around 0.2 µm, with 90 s deposition time at 60°C. We also conducted deposition with larger $Cu(NO_3)_2$ concentrations (5 mM and 10 mM); however, the thickness decreased and became nonuniform; therefore, those samples were not subjected to any further characterization.
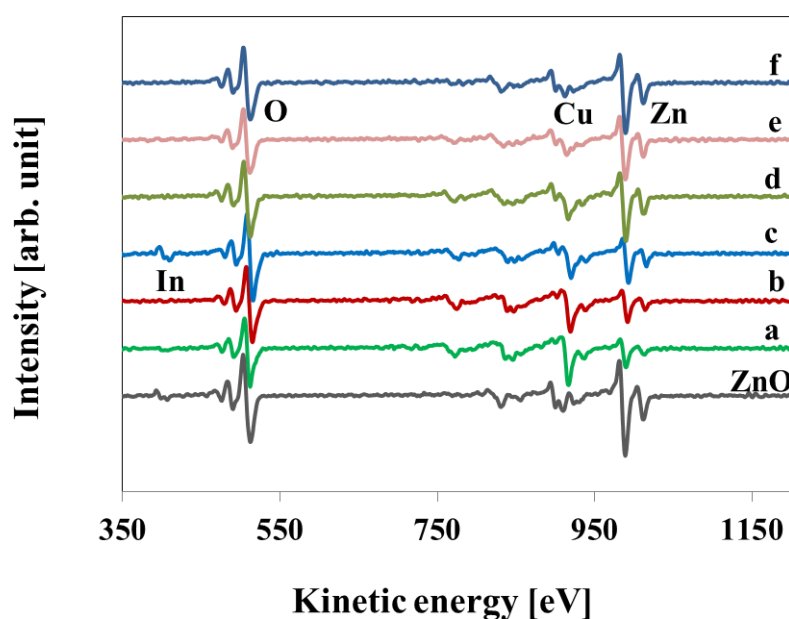

Figure 4. AES spectra for the samples fabricated with 1 mM $Cu(NO_3)_2$ and $Zn(NO_3)_2$ concentrations of (a) 5 mM, (b) 10 mM, and (c) 20 mM (at RT), and (d) 5 mM, (e) 10 mM, and (f) 20 mM (at 60°C).

Fig. 4 illustrates AES spectra for the (CuZn)O films fabricated with 1 mM $Cu(NO_3)_2$ and various concentrations of $Zn(NO_3)_2$. The $Zn(NO_3)_2$ concentration and deposition time are as follows: (a) 5 mM, 210 s; (b) 10 mM, 150 s; (c) 20 mM, 270 s; (d) 5 mM, 150 s; (e) 10 mM, 90 s; and (f) 20 mM, 90 s. The deposition temperature is RT for (a)–(c) and 60°C for (d)–(f). In these spectra, the dominant signals are assigned to Zn, Cu, and O, as long as a small signal is assigned to In

Fig. 5 shows the elemental composition ration of (CuZn)O for the samples obtained from the AES peak intensities at different concentrations of $Zn(NO_3)_2$ and tested at the two different bath temperatures. The Cu/Zn ratios for the samples fabricated at RT are between 2 and 0.85, and they significantly decrease. For the films deposited at 60°C, they are in a range between 0.49 and 0.19.
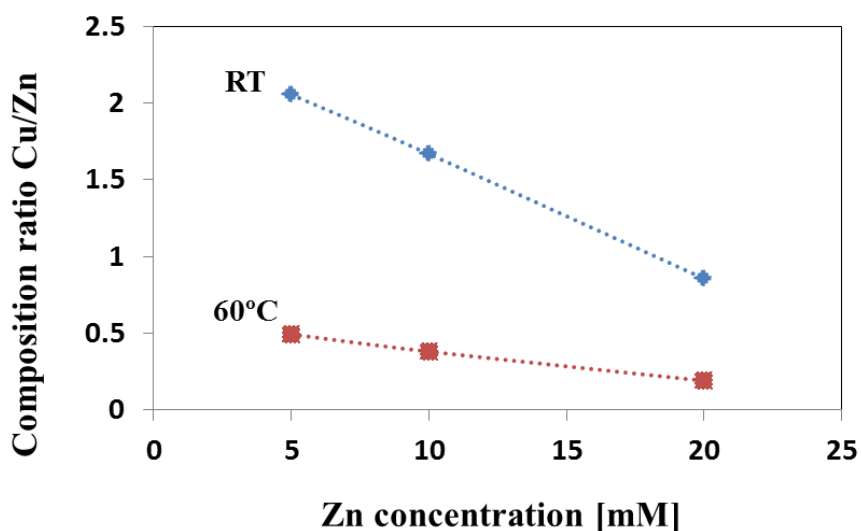

Figure 5. Cu/Zn composition ratio for samples obtained with various $Zn(NO_3)_2$ concentrations and tested at two different bath temperatures.

The SEM images for the samples fabricated at various temperatures and $Zn(NO_3)_2$ concentrations are presented in Fig. 6. The $Zn(NO_3)_2$ concentration and deposition times are as follows: (a) 5 mM, 210 s; (b) 10 mM, 150 s; (c) 20 mM, 270 s; (d) 5 mM, 150 s; (e) 10 mM, 90 s; and (f) 20 mM, 90 s. The deposition time for ZnO is 210 s. The fabrication temperature is RT for (a)–(c) and 60°C for (d)–(f). The pure ZnO sample exhibits larger particle size with an average diameter of ~500 nm, whereas with Cu doping, uniform and smaller grains (of approximately 200 nm) were observed on a continuous film. This confirms that Cu ions will decrease the grain size of ZnO [21]. For the (CuZn)O samples, there is no meaningful difference in morphology due to variation in deposition temperature or $Zn(NO_3)_2$ concentration.
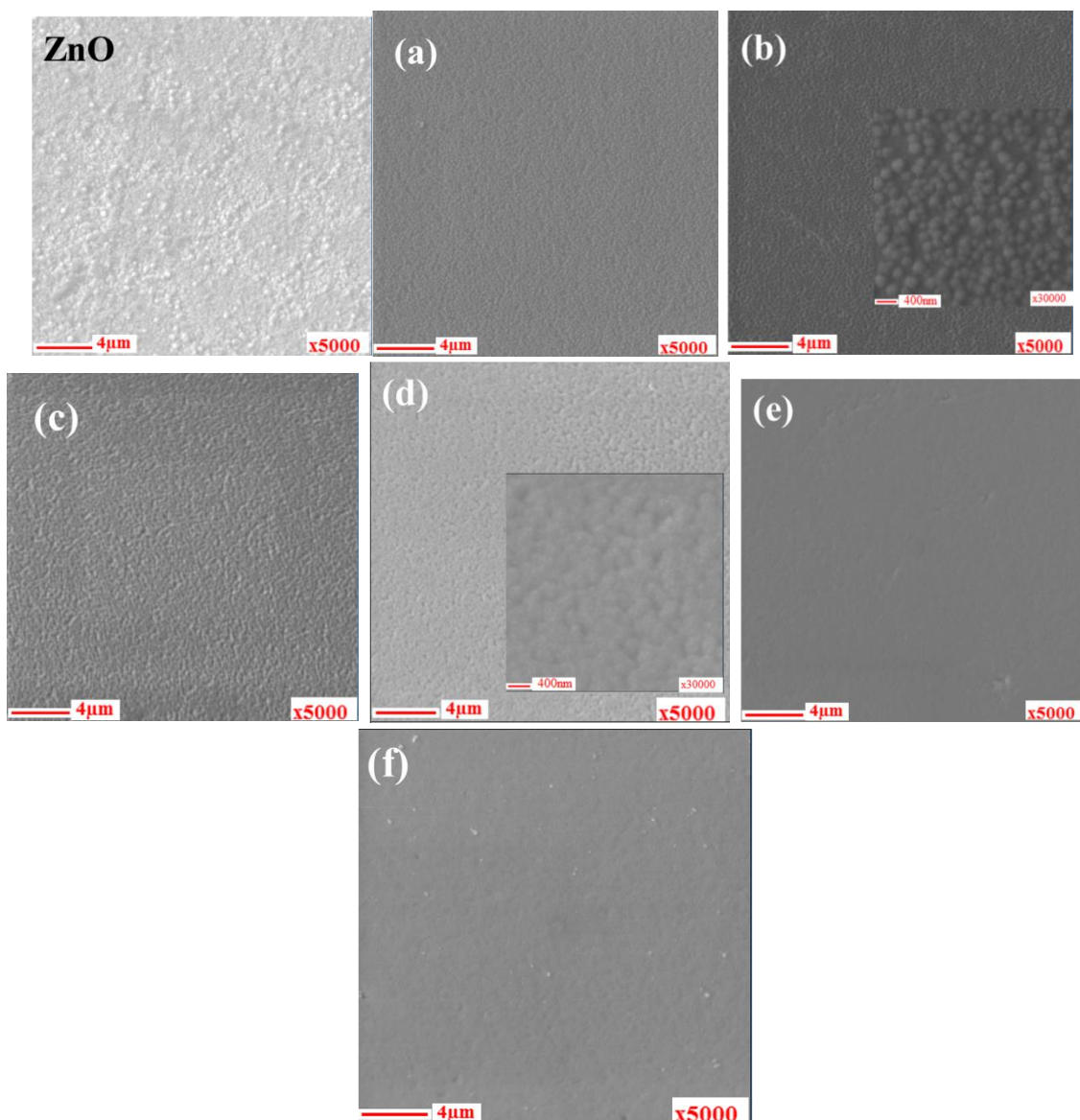
Figure 6. SEM photographs for the samples fabricated with 1 mM Cu(NO$_3$)$_2$ and Zn(NO$_3$)$_2$ concentration of (a) 5 mM, (b) 10 mM, and (c) 20 mM (at RT); and (d) 5 mM, (e) 10 mM, and (f) 20 mM (at 60°C).

Figs. 7 (a) and (b) show XRD patterns for the films fabricated at RT and 60°C, respectively. Fig. 7 (a) illustrates the XRD patterns for the ITO substrate and the sample deposited with 1 mM Cu(NO$_3$)$_2$ and 5 mM Zn(NO$_3$)$_2$. We observed no peaks other than those for ITO, and there were no XRD peaks for the other films fabricated at RT. These results reveal that the samples fabricated at RT are dominantly amorphous. For the samples fabricated at 60°C, the diffraction peaks of ZnO were observed and indexed in Fig. 7 (b). The weak preferential orientation in (002) was observed for the (CuZn)O sample and not for pure ZnO. There is no shift in peak position compared with ZnO, and no additional peaks corresponding to Cu were detected. Therefore, the hexagonal wurtzite structure of ZnO was not modified by Cu ions.
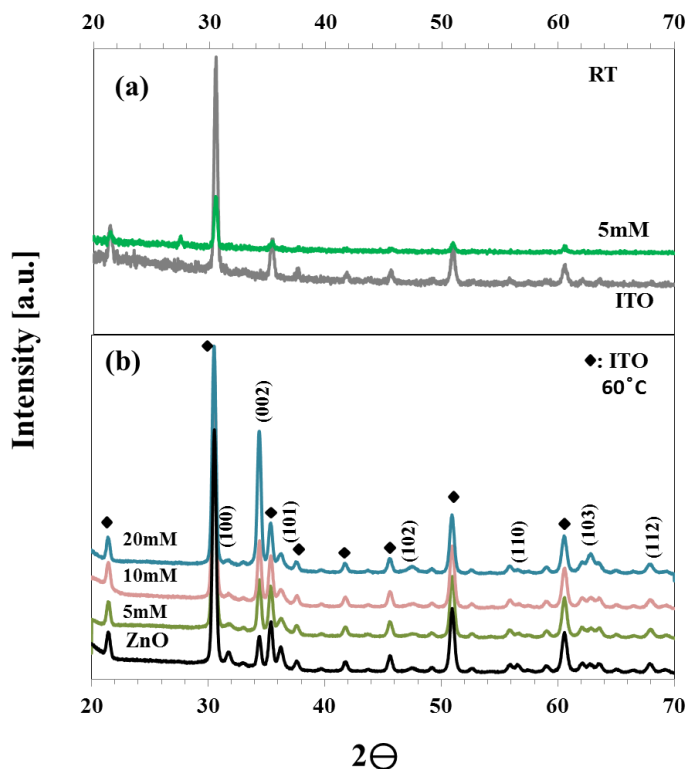
Figure 7. XRD patterns of the samples fabricated at (a) RT and (b) 60°C, with 1 mM Cu(NO₃)₂ and different Zn(NO₃)₂ concentrations.

.

Fig. 8(a) presents the optical transmission spectra for the films fabricated with various $Zn(NO_3)_2$ concentrations and different deposition temperatures. The films have transparency of more than 65% in the visible regions, and the transmittance tends to decrease with reductions in the quantity of $Zn(NO_3)_2$. As noted above, the samples fabricated at 60°C are thicker than those deposited at RT. An obvious absorption edge was confirmed for the samples deposited at 60°C, whereas for the samples fabricated at RT, the transmittance decreased only gradually in the UV range with decreasing wavelength.

Fig. 8(b) shows estimation of the band gap from the plot of $(\alpha h\nu)^2$ vs. $h\nu$, where $h\nu$ is photon energy and α the absorption coefficient. The band gap was found to be 3.5 eV in undoped ZnO deposited at 60°C. The band gap became smaller with the decreasing $Zn(NO_3)_2$ concentration, i.e., with the increasing Cu/Zn ratio. Band gap narrowing of (CuZn)O with Cu content has been reported previously [5,14,15,17,20,23]. For the samples deposited at RT, as the absorption edge does not appear obviously, the band gap cannot be exactly calculated. However, it is possible to see that with the increasing $Zn(NO_3)_2$ concentration or decreasing Cu/Zn ratio, the band gap increases. The absorption edge seems to shift to shorter wavelengths by decreasing deposition temperature; the transmittance in the UV range is higher for the films deposited at RT.
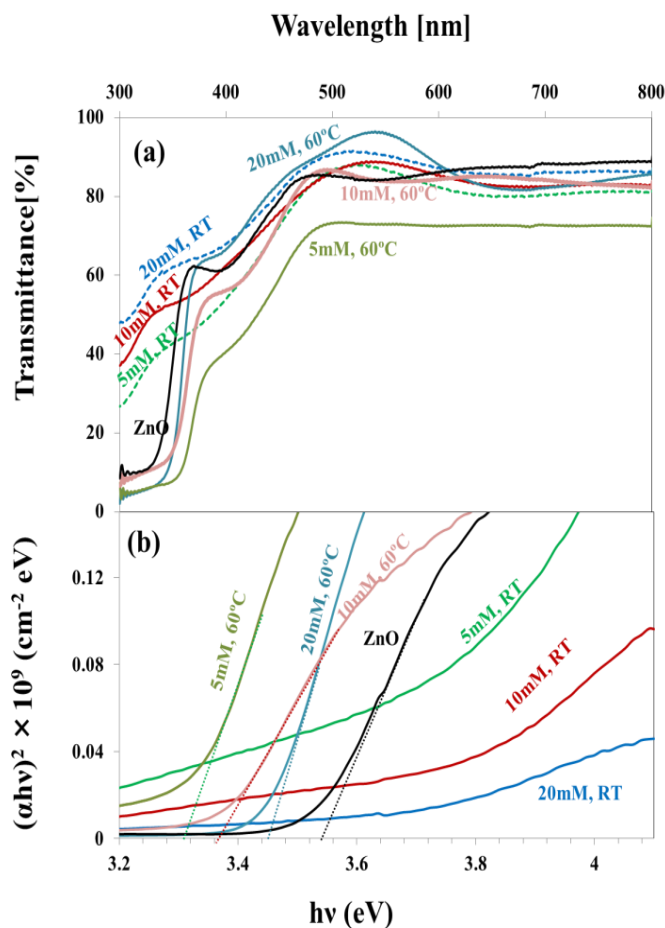
Figure 8. (a) Optical transmittance of the films deposited with 1 mM $Cu(NO_3)_2$ and different $Zn(NO_3)_2$ concentrations and different temperatures and (b) Plots of $(\alpha h\nu)^2$ vs. $h\nu$.

Figs. 9 (a) and (b) illustrate the PEC measurement results for the samples fabricated at RT and 60°C, respectively. For the samples deposited at RT (Fig. 9(a)), clear photo response was observed in the negative part, which means that the electron is the minority carrier, i.e., those films have p-type conductivity. In contrast, in Fig. 9(b), the positive photocurrent appeared for ZnO, indicating n-type conductivity. The positive response is dominant for the film fabricated with 20 mM $Zn(NO_3)_2$. For the films fabricated with 5 and 10 mM of $Zn(NO_3)_2$, both the negative and positive photocurrent responses were observed, and therefore the conduction type would be near to intrinsic.
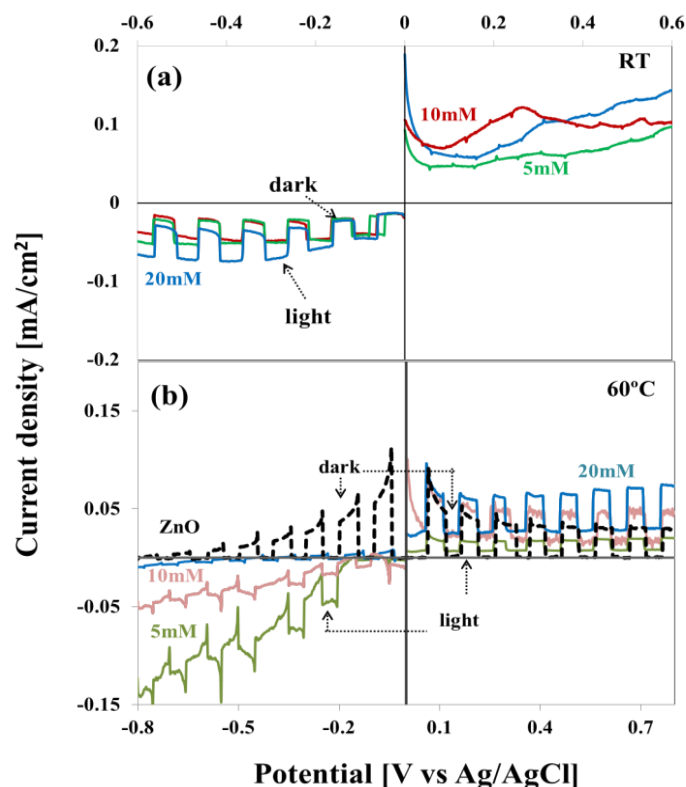
Figure 9. Photocurrent responses in the PEC measurements for the samples deposited at (a) RT and (b) 60°C, with 1 mM $Cu(NO_3)_2$ and different $Zn(NO_3)_2$ concentrations.

4. DISCUSSION

In this study, we fabricated (CuZn)O thin films at RT and 60°C and found that for the same deposition solution and potential, the deposition current is smaller at RT than at 60°C. In addition, the Cu/Zn ratio is significantly higher at RT than at 60°C. Thus, the deposition of ZnO is enhanced by heating the deposition solution.

Since copper oxides have a smaller band gap than ZnO, introduction of Cu into ZnO is considered to reduce the band gap of ZnO. Indeed, band gap reduction by Cu doping has been previously reported [5,14,15,17,20,23]. However, the (CuZn)O films deposited at RT have high transparency in the visible-UV region, although the Cu/Zn is larger than unity. We can exclude the possibility that Cu_2O was deposited because Cu_2O is not transparent in visible light. The high transparency could be partly associated with the formation of $Zn(OH)_2$, which has a larger band gap than ZnO. Furthermore, we can consider the effects of different morphology (shown in Fig. 6) on light scattering. Based on the XRD patterns, the samples fabricated at RT are amorphous, whereas those deposited at 60°C are polycrystalline. The amorphous nature leads to the absence of a clear absorption edge and higher transparency in the UV range for the RT deposited samples [25]. The hexagonal wurtzite phase of ZnO, formed in the films deposited at 60°C, is known to be the most stable phase of ZnO [3,26,27].

The (CuZn)O films deposited at RT were p-type, whereas the films deposited at 60°C were n-type or nearly intrinsic because the Cu/Zn ratio is larger for the RT deposited samples. The amorphous

(CuZn)O deposited at RT has high transparency in the visible regions and exhibits clear p-type photo response. Thus, it is expected that it will be applied to optoelectronic devices in transparent electronics, such as transparent p–n junction solar cells.

5. CONCLUSIONS

(CuZn)O thin films have been prepared by potentiostatic ECD with constant concentrations of $Cu(NO_3)_2$ and various concentrations of $Zn(NO_3)_2$. The XRD results demonstrated that the (CuZn)O films deposited at RT are amorphous. The photo-spectroscopy revealed a high transmittance (>65%) in the visible region, and the PEC measurement indicated that p-type conductivity. In contrast, for the films deposited at 60°C, XRD peaks attributed to wurtzite ZnO were observed. The optical band gap was found to be in the range of 3.25–3.49 eV, and the conduction type was n-type or nearly intrinsic. Thus, through using ECD at RT, we obtained transparent p-type films, which are essential for p–n junction devices in transparent electronics.

References

1. S.C. Lyu, Y. Zhang, H. Ruh, H.-J. Lee, H.-W. Shim, E.-K. Suh, and C.J. Lee, *Chem. Phys. Lett.*, 363 (2002) 134.
2. L.-C Chen, C.-A. Hsieh, and X. Zhang, *Materials*, 7 (2014) 7304.
3. T. P. Rao, M.C. S. Kumar, S. A. Angayarkanni, and M. Ashok, *J. Alloys Compd,* 485 (2009) 413.
4. M.B. Rahmani, S.H. Keshmiri, M. Shafiei, K. Latham, W. Wlodarski, J. du Plessis, and K. Kalantar-Zadeh, *Sens. Lett.*, 7 (2009) 1.
5. C. Xia, F. Wang, and C. Hu, *J. Alloys Compd*, 589 (2014) 604.
6. B. Allabergenov, O. Tursunkulov, A.I. Abidov, C. Byeongdae, J.S. Wook, and S. Kim, *J. Cryst. Growth.*, 401 (2014) 573.
7. M. Wang, L. Jiang, E.J. Kim, and S.H. Hahn, *RSC Adv.*, 5 (2015) 87496.
8. M. Karakawa, T. Sugahara, Y. Hirose, K. Suganuma, and Y. Aso, *Sci. Rep*, 8 (2018) 10839.
9. X.-R. Qu and D.-C. Jia, *J. Cryst. Growth.*, 311 (2009) 1223.
10. S.-S. Xu, H.-L. Lu , Y. Zhang, T. Wang, Y. Geng, W. Huang, S.-J. Ding, and D.W. Zhang, *J. Alloys Compd.*, 638 (2015) 133.
11. Y. Yan, M.M. Al-Jassim, and S.-H. Wei, *Appl. Phys. Lett.,* 89 (2006) 181912.
12. F. Ghahramanifard, A. Rouhollahi , and O. Fazlolahzadeh, *Superlattic. Microt*, 114 (2018) 1.
13. S.B. Zhang, S.-H. Wei, and A. Zunger, *Phys. Rev. B*, 63 (2001) 075205.
14. M. Mittal, M. Sharma, and O.P. Pandey, *Sol. Energy,* 110 (2014) 386.
15. R.-C. Wang, and H.-Y. Lin, Mater. *Chem. Phys.*, 125 (2011) 263.
16. M. Fu, Y. Li, S. Wu, P. Lu, J. Liu, and F. Dong, *Appl. Surf. Sci.*, 258 (2011) 1587.
17. R. Mohan, K. Krishnamoorthy, and S.-J. Kim, *Solid State Commun.*, 152 (2012) 375.
18. S.A. Nasser, H.H. Afify, S. A. El-Hakim, and M.K. Zayed, *Thin Solid Films*, 315 (1998) 327.
19. Q. A. Drmosh, S. G. Rao, Z. H. Yamani, and M. A. Gondal, *Appl. Surf. Sci.,* 270 (2013) 104.
20. K.-S. Ahn, T. Deutsch, Y. Yan, C.-S. Jiang, C. L. Perkins, J. Turner, and M. Al-Jassim, *J. Appl. Phys.,* 102 (2007) 023517.
21. H.L. Pan, B. Yao, T. Xu, B.Y. Zhang, W.W. Liu, and D. Z. Shen, *Appl. Phys. Let.*, 97 (2010) 142101.

22. C. Chen, W. Dai, Y. Lu, H. He, Q. Lu, T. Jin, and Z. Ye, *Mater. Res. Bull.,* 70 (2015) 190.
23. O. Lupan, T. Pauporte, B. Viana, and P. Aschehoug, *Electrochim. Acta*, 56 (2011)10543.
24. L. Mentar, H. Lahmar, M.R. Khelladi, and A. Azizi, *J. New Technol. Mater.,* 04 (2014) 41.
25. H.X. Deng, S.H. Wei, S.S. Li, J. Li, and A. Walsh, *Phys. Rev. B*, 87 (2013) 12503.
26. M. Kumar, and C. Sasikumar, *Am. J. Mater. Sci.,* 2 (2014) 18.
27. M. Babikier, D. Wang, J. Wang, Q. Li, J. Sun, Y. Yan, Q. Yu, and S. Jiao, *Nanoscale Res. Lett.,* 9 (2014) 1.